Measurement of the *CP*-even fraction of $D^0 \to K^+K^-\pi^+\pi^-$

M. Ablikim,[1] M. N. Achasov,[12,b] P. Adlarson,[72] M. Albrecht,[4] R. Aliberti,[33] A. Amoroso,[71a,71c] M. R. An,[37] Q. An,[68,55] Y. Bai,[54] O. Bakina,[34] R. Baldini Ferroli,[27a] I. Balossino,[28a] Y. Ban,[44,g] V. Batozskaya,[1,42] D. Becker,[33] K. Begzsuren,[30] N. Berger,[33] M. Bertani,[27a] D. Bettoni,[28a] F. Bianchi,[71a,71c] E. Bianco,[71a,71c] J. Bloms,[65] A. Bortone,[71a,71c] I. Boyko,[34] R. A. Briere,[5] A. Brueggemann,[65] H. Cai,[73] X. Cai,[1,55] A. Calcaterra,[27a] G. F. Cao,[1,60] N. Cao,[1,60] S. A. Cetin,[59a] J. F. Chang,[1,55] W. L. Chang,[1,60] G. R. Che,[41] G. Chelkov,[34,a] C. Chen,[41] Chao Chen,[52] G. Chen,[1] H. S. Chen,[1,60] M. L. Chen,[1,55,60] S. J. Chen,[40] S. M. Chen,[58] T. Chen,[1,60] X. R. Chen,[29,60] X. T. Chen,[1,60] Y. B. Chen,[1,55] Z. J. Chen,[24,h] W. S. Cheng,[71c] S. K. Choi,[52] X. Chu,[41] G. Cibinetto,[28a] F. Cossio,[71c] J. J. Cui,[47] H. L. Dai,[1,55] J. P. Dai,[76] A. Dbeyssi,[18] R. E. de Boer,[4] D. Dedovich,[34] Z. Y. Deng,[1] A. Denig,[33] I. Denysenko,[34] M. Destefanis,[71a,71c] F. De Mori,[71a,71c] Y. Ding,[32] Y. Ding,[38] J. Dong,[1,55] L. Y. Dong,[1,60] M. Y. Dong,[1,55,60] X. Dong,[73] S. X. Du,[78] Z. H. Duan,[40] P. Egorov,[34,a] Y. L. Fan,[73] J. Fang,[1,55] S. S. Fang,[1,60] W. X. Fang,[1] Y. Fang,[1] R. Farinelli,[28a] L. Fava,[71b,71c] F. Feldbauer,[4] G. Felici,[27a] C. Q. Feng,[68,55] J. H. Feng,[56] K Fischer,[66] M. Fritsch,[4] C. Fritzsch,[65] C. D. Fu,[1] H. Gao,[60] Y. N. Gao,[44,g] Yang Gao,[68,55] S. Garbolino,[71c] I. Garzia,[28a,28b] P. T. Ge,[73] Z. W. Ge,[40] C. Geng,[56] E. M. Gersabeck,[64] A Gilman,[66] K. Goetzen,[13] L. Gong,[38] W. X. Gong,[1,55] W. Gradl,[33] M. Greco,[71a,71c] L. M. Gu,[40] M. H. Gu,[1,55] Y. T. Gu,[15] C. Y Guan,[1,60] A. Q. Guo,[29,60] L. B. Guo,[39] R. P. Guo,[46] Y. P. Guo,[11,f] A. Guskov,[34,a] W. Y. Han,[37] X. Q. Hao,[19] F. A. Harris,[62] K. K. He,[52] K. L. He,[1,60] F. H. Heinsius,[4] C. H. Heinz,[33] Y. K. Heng,[1,55,60] C. Herold,[57] G. Y. Hou,[1,60] Y. R. Hou,[60] Z. L. Hou,[1] H. M. Hu,[1,60] J. F. Hu,[53,i] T. Hu,[1,55,60] Y. Hu,[1] G. S. Huang,[68,55] K. X. Huang,[56] L. Q. Huang,[29,60] X. T. Huang,[47] Y. P. Huang,[1] Z. Huang,[44,g] T. Hussain,[70] N Hüsken,[26,33] W. Imoehl,[26] M. Irshad,[68,55] J. Jackson,[26] S. Jaeger,[4] S. Janchiv,[30] E. Jang,[52] J. H. Jeong,[52] Q. Ji,[1] Q. P. Ji,[19] X. B. Ji,[1,60] X. L. Ji,[1,55] Y. Y. Ji,[47] Z. K. Jia,[68,55] P. C. Jiang,[44,g] S. S. Jiang,[37] X. S. Jiang,[1,55,60] Y. Jiang,[60] J. B. Jiao,[47] Z. Jiao,[22] S. Jin,[40] Y. Jin,[63] M. Q. Jing,[1,60] T. Johansson,[72] S. Kabana,[31] N. Kalantar-Nayestanaki,[61] X. L. Kang,[9] X. S. Kang,[38] R. Kappert,[61] M. Kavatsyuk,[61] B. C. Ke,[78] I. K. Keshk,[4] A. Khoukaz,[65] R. Kiuchi,[1] R. Kliemt,[13] L. Koch,[35] O. B. Kolcu,[59a] B. Kopf,[4] M. Kuemmel,[4] M. Kuessner,[4] A. Kupsc,[42,72] W. Kühn,[35] J. J. Lane,[64] J. S. Lange,[35] P. Larin,[18] A. Lavania,[25] L. Lavezzi,[71a,71c] T. T. Lei,[68,k] Z. H. Lei,[68,55] H. Leithoff,[33] M. Lellmann,[33] T. Lenz,[33] C. Li,[45] C. Li,[41] C. H. Li,[37] Cheng Li,[68,55] D. M. Li,[78] F. Li,[1,55] G. Li,[1] H. Li,[68,55] H. B. Li,[1,60] H. J. Li,[19] H. N. Li,[53,i] Hui Li,[41] J. Q. Li,[4] J. S. Li,[56] J. W. Li,[47] Ke Li,[1] L. J Li,[1,60] L. K. Li,[1] Lei Li,[3] M. H. Li,[41] P. R. Li,[36,j,k] S. X. Li,[11] S. Y. Li,[58] T. Li,[47] W. D. Li,[1,60] W. G. Li,[1] X. H. Li,[68,55] X. L. Li,[47] Xiaoyu Li,[1,60] Y. G. Li,[44,g] Z. X. Li,[15] Z. Y. Li,[56] C. Liang,[40] H. Liang,[32] H. Liang,[68,55] H. Liang,[1,60] Y. F. Liang,[51] Y. T. Liang,[29,60] G. R. Liao,[14] L. Z. Liao,[47] J. Libby,[25] A. Limphirat,[57] C. X. Lin,[56] D. X. Lin,[29,60] T. Lin,[1] B. J. Liu,[1] C. Liu,[32] C. X. Liu,[1] D. Liu,[18,68] F. H. Liu,[50] Fang Liu,[1] Feng Liu,[6] G. M. Liu,[53,i] H. Liu,[36,j,k] H. B. Liu,[15] H. M. Liu,[1,60] Huanhuan Liu,[1] Huihui Liu,[20] J. B. Liu,[68,55] J. L. Liu,[69] J. Y. Liu,[1,60] K. Liu,[1] K. Y. Liu,[38] Ke Liu,[21] L. Liu,[68,55] L. C. Liu,[21] Lu Liu,[41] M. H. Liu,[11,f] P. L. Liu,[1] Q. Liu,[60] S. B. Liu,[68,55] T. Liu,[11,f] W. K. Liu,[41] W. M. Liu,[68,55] X. Liu,[36,j,k] Y. Liu,[36,j,k] Y. B. Liu,[41] Z. A. Liu,[1,55,60] Z. Q. Liu,[47] X. C. Lou,[1,55,60] F. X. Lu,[56] H. J. Lu,[22] J. G. Lu,[1,55] X. L. Lu,[1] Y. Lu,[7] Y. P. Lu,[1,55] Z. H. Lu,[1,60] C. L. Luo,[39] M. X. Luo,[77] T. Luo,[11,f] X. L. Luo,[1,55] X. R. Lyu,[60] Y. F. Lyu,[41] F. C. Ma,[38] H. L. Ma,[1] L. L. Ma,[47] M. M. Ma,[1,60] Q. M. Ma,[1] R. Q. Ma,[1,60] R. T. Ma,[60] X. Y. Ma,[1,55] Y. Ma,[44,g] F. E. Maas,[18] M. Maggiora,[71a,71c] S. Maldaner,[4] S. Malde,[66] Q. A. Malik,[70] A. Mangoni,[27b] Y. J. Mao,[44,g] Z. P. Mao,[1] S. Marcello,[71a,71c] Z. X. Meng,[63] J. G. Messchendorp,[13,61] G. Mezzadri,[28a] H. Miao,[1,60] T. J. Min,[40] R. E. Mitchell,[26] X. H. Mo,[1,55,60] N. Yu. Muchnoi,[12,b] Y. Nefedov,[34] F. Nerling,[18,d] I. B. Nikolaev,[12,b] Z. Ning,[1,55] S. Nisar,[10,l] Y. Niu,[47] S. L. Olsen,[60] Q. Ouyang,[1,55,60] S. Pacetti,[27b,27c] X. Pan,[52] Y. Pan,[54] A. Pathak,[32] Y. P. Pei,[68,55] M. Pelizaeus,[4] H. P. Peng,[68,55] K. Peters,[13,d] J. L. Ping,[39] R. G. Ping,[1,60] S. Plura,[33] S. Pogodin,[34] V. Prasad,[68,55] F. Z. Qi,[1] H. Qi,[68,55] H. R. Qi,[58] M. Qi,[40] T. Y. Qi,[11,f] S. Qian,[1,55] W. B. Qian,[60] Z. Qian,[56] C. F. Qiao,[60] J. J. Qin,[69] L. Q. Qin,[14] X. P. Qin,[11,f] X. S. Qin,[47] Z. H. Qin,[1,55] J. F. Qiu,[1] S. Q. Qu,[58] K. H. Rashid,[70] C. F. Redmer,[33] K. J. Ren,[37] A. Rivetti,[71c] V. Rodin,[61] M. Rolo,[71c] G. Rong,[1,60] Ch. Rosner,[18] S. N. Ruan,[41] A. Sarantsev,[34,c] Y. Schelhaas,[33] C. Schnier,[4] K. Schoenning,[72] M. Scodeggio,[28a,28b] K. Y. Shan,[11,f] W. Shan,[23] X. Y. Shan,[68,55] J. F. Shangguan,[52] L. G. Shao,[1,60] M. Shao,[68,55] C. P. Shen,[11,f] H. F. Shen,[1,60] W. H. Shen,[60] X. Y. Shen,[1,60] B. A. Shi,[60] H. C. Shi,[68,55] J. Y. Shi,[1] Q. Q. Shi,[52] R. S. Shi,[1,60] X. Shi,[1,55] J. J. Song,[19] W. M. Song,[32,1] Y. X. Song,[44,g] S. Sosio,[71a,71c] S. Spataro,[71a,71c] F. Stieler,[33] P. P. Su,[52] Y. J. Su,[60] G. X. Sun,[1] H. Sun,[60] H. K. Sun,[1] J. F. Sun,[19] L. Sun,[73] S. S. Sun,[1,60] T. Sun,[1,60] W. Y. Sun,[32] Y. J. Sun,[68,55] Y. Z. Sun,[1] Z. T. Sun,[47] Y. X. Tan,[68,55] C. J. Tang,[51] G. Y. Tang,[1] J. Tang,[56] Y. A. Tang,[73] L. Y Tao,[69] Q. T. Tao,[24,h] M. Tat,[66] J. X. Teng,[68,55] V. Thoren,[72] W. H. Tian,[49] Y. Tian,[29,60] I. Uman,[59b] B. Wang,[68,55] B. Wang,[1] B. L. Wang,[60] C. W. Wang,[40] D. Y. Wang,[44,g] F. Wang,[69] H. J. Wang,[36,j,k] H. P. Wang,[1,60] K. Wang,[1,55] L. L. Wang,[1] M. Wang,[47] Meng Wang,[1,60] S. Wang,[11,f] S. Wang,[14] T. Wang,[11,f] T. J. Wang,[41] W. Wang,[56] W. H. Wang,[73] W. P. Wang,[68,55] X. Wang,[44,g] X. F. Wang,[36,j,k] X. L. Wang,[11,f] Y. Wang,[58] Y. D. Wang,[43] Y. F. Wang,[1,55,60] Y. H. Wang,[45] Y. Q. Wang,[1] Yaqian Wang,[17,1] Z. Wang,[1,55] Z. Y. Wang,[1,60] Ziyi Wang,[60] D. H. Wei,[14] F. Weidner,[65] S. P. Wen,[1] D. J. White,[64] U. Wiedner,[4] G. Wilkinson,[66] M. Wolke,[72] L. Wollenberg,[4] J. F. Wu,[1,60] L. H. Wu,[1] L. J. Wu,[1,60] X. Wu,[11,f] X. H. Wu,[32] Y. Wu,[68] Y. J Wu,[29] Z. Wu,[1,55] L. Xia,[68,55] T. Xiang,[44,g] D. Xiao,[36,j,k] G. Y. Xiao,[40] H. Xiao,[11,f] S. Y. Xiao,[1] Y. L. Xiao,[11,f] Z. J. Xiao,[39] C. Xie,[40] X. H. Xie,[44,g] Y. Xie,[47] Y. G. Xie,[1,55] Y. H. Xie,[6] Z. P. Xie,[68,55]

T. Y. Xing,[1,60] C. F. Xu,[1,60] C. J. Xu,[56] G. F. Xu,[1] H. Y. Xu,[63] Q. J. Xu,[16] X. P. Xu,[52] Y. C. Xu,[75] Z. P. Xu,[40] F. Yan,[11,f]
L. Yan,[11,f] W. B. Yan,[68,55] W. C. Yan,[78] H. J. Yang,[48,e] H. L. Yang,[32] H. X. Yang,[1] Tao Yang,[1] Y. F. Yang,[41] Y. X. Yang,[1,60]
Yifan Yang,[1,60] M. Ye,[1,55] M. H. Ye,[8] J. H. Yin,[1] Z. Y. You,[56] B. X. Yu,[1,55,60] C. X. Yu,[41] G. Yu,[1,60] T. Yu,[69] X. D. Yu,[44,g]
C. Z. Yuan,[1,60] L. Yuan,[2] S. C. Yuan,[1] X. Q. Yuan,[1] Y. Yuan,[1,60] Z. Y. Yuan,[56] C. X. Yue,[37] A. A. Zafar,[70] F. R. Zeng,[47]
X. Zeng,[6] Y. Zeng,[24,h] X. Y. Zhai,[32] Y. H. Zhan,[56] A. Q. Zhang,[1,60] B. L. Zhang,[1,60] B. X. Zhang,[1] D. H. Zhang,[41]
G. Y. Zhang,[19] H. Zhang,[68] H. H. Zhang,[32] H. H. Zhang,[56] H. Q. Zhang,[1,55,60] H. Y. Zhang,[1,55] J. J. Zhang,[49] J. L. Zhang,[74]
J. Q. Zhang,[39] J. W. Zhang,[1,55,60] J. X. Zhang,[36,j,k] J. Y. Zhang,[1] J. Z. Zhang,[1,60] Jianyu Zhang,[1,60] Jiawei Zhang,[1,60]
L. M. Zhang,[58] L. Q. Zhang,[56] Lei Zhang,[40] P. Zhang,[1] Q. Y. Zhang,[37,78] Shuihan Zhang,[1,60] Shulei Zhang,[24,h]
X. D. Zhang,[43] X. M. Zhang,[1] X. Y. Zhang,[47] X. Y. Zhang,[52] Y. Zhang,[66] Y. T. Zhang,[78] Y. H. Zhang,[1,55] Yan Zhang,[68,55]
Yao Zhang,[1] Z. H. Zhang,[1] Z. L. Zhang,[32] Z. Y. Zhang,[41] Z. Y. Zhang,[73] G. Zhao,[1] J. Y. Zhao,[1,60] J. Z. Zhao,[1,55]
Lei Zhao,[68,55] Ling Zhao,[1] M. G. Zhao,[41] S. J. Zhao,[78] Y. B. Zhao,[1,55] Y. X. Zhao,[29,60] Z. G. Zhao,[68,55] A. Zhemchugov,[34,a]
B. Zheng,[69] J. P. Zheng,[1,55] Y. H. Zheng,[60] B. Zhong,[39] C. Zhong,[69] X. Zhong,[56] H. Zhou,[47] L. P. Zhou,[1,60] X. Zhou,[73]
X. K. Zhou,[60] X. R. Zhou,[68,55] X. Y. Zhou,[37] Y. Z. Zhou,[11,f] J. Zhu,[41] K. Zhu,[1] K. J. Zhu,[1,55,60] L. X. Zhu,[60] S. H. Zhu,[67]
S. Q. Zhu,[40] W. J. Zhu,[11,f] Y. C. Zhu,[68,55] Z. A. Zhu,[1,60] J. H. Zou,[1] and J. Zu[68,55]

(BESIII Collaboration)

[1]*Institute of High Energy Physics, Beijing 100049, People's Republic of China*
[2]*Beihang University, Beijing 100191, People's Republic of China*
[3]*Beijing Institute of Petrochemical Technology, Beijing 102617, People's Republic of China*
[4]*Bochum Ruhr-University, D-44780 Bochum, Germany*
[5]*Carnegie Mellon University, Pittsburgh, Pennsylvania 15213, USA*
[6]*Central China Normal University, Wuhan 430079, People's Republic of China*
[7]*Central South University, Changsha 410083, People's Republic of China*
[8]*China Center of Advanced Science and Technology, Beijing 100190, People's Republic of China*
[9]*China University of Geosciences, Wuhan 430074, People's Republic of China*
[10]*COMSATS University Islamabad, Lahore Campus,*
Defence Road, Off Raiwind Road, 54000 Lahore, Pakistan
[11]*Fudan University, Shanghai 200433, People's Republic of China*
[12]*Budker Institute of Nuclear Physics SB RAS (BINP), Novosibirsk 630090, Russia*
[13]*GSI Helmholtzcentre for Heavy Ion Research GmbH, D-64291 Darmstadt, Germany*
[14]*Guangxi Normal University, Guilin 541004, People's Republic of China*
[15]*Guangxi University, Nanning 530004, People's Republic of China*
[16]*Hangzhou Normal University, Hangzhou 310036, People's Republic of China*
[17]*Hebei University, Baoding 071002, People's Republic of China*
[18]*Helmholtz Institute Mainz, Staudinger Weg 18, D-55099 Mainz, Germany*
[19]*Henan Normal University, Xinxiang 453007, People's Republic of China*
[20]*Henan University of Science and Technology, Luoyang 471003, People's Republic of China*
[21]*Henan University of Technology, Zhengzhou 450001, People's Republic of China*
[22]*Huangshan College, Huangshan 245000, People's Republic of China*
[23]*Hunan Normal University, Changsha 410081, People's Republic of China*
[24]*Hunan University, Changsha 410082, People's Republic of China*
[25]*Indian Institute of Technology Madras, Chennai 600036, India*
[26]*Indiana University, Bloomington, Indiana 47405, USA*
[27a]*INFN Laboratori Nazionali di Frascati, I-00044 Frascati, Italy*
[27b]*INFN Sezione di Perugia, I-06100 Perugia, Italy*
[27c]*University of Perugia, I-06100 Perugia, Italy*
[28a]*INFN Sezione di Ferrara, I-44122 Ferrara, Italy*
[28b]*University of Ferrara, I-44122 Ferrara, Italy*
[29]*Institute of Modern Physics, Lanzhou 730000, People's Republic of China*
[30]*Institute of Physics and Technology, Peace Avenue 54B, Ulaanbaatar 13330, Mongolia*
[31]*Instituto de Alta Investigación, Universidad de Tarapacá, Casilla 7D, Arica 1000000, Chile*
[32]*Jilin University, Changchun 130012, People's Republic of China*
[33]*Johannes Gutenberg University of Mainz, Johann-Joachim-Becher-Weg 45, D-55099 Mainz, Germany*
[34]*Joint Institute for Nuclear Research, 141980 Dubna, Moscow region, Russia*
[35]*Justus-Liebig-Universitaet Giessen, II. Physikalisches Institut,*
Heinrich-Buff-Ring 16, D-35392 Giessen, Germany
[36]*Lanzhou University, Lanzhou 730000, People's Republic of China*
[37]*Liaoning Normal University, Dalian 116029, People's Republic of China*

[38]*Liaoning University, Shenyang 110036, People's Republic of China*
[39]*Nanjing Normal University, Nanjing 210023, People's Republic of China*
[40]*Nanjing University, Nanjing 210093, People's Republic of China*
[41]*Nankai University, Tianjin 300071, People's Republic of China*
[42]*National Centre for Nuclear Research, Warsaw 02-093, Poland*
[43]*North China Electric Power University, Beijing 102206, People's Republic of China*
[44]*Peking University, Beijing 100871, People's Republic of China*
[45]*Qufu Normal University, Qufu 273165, People's Republic of China*
[46]*Shandong Normal University, Jinan 250014, People's Republic of China*
[47]*Shandong University, Jinan 250100, People's Republic of China*
[48]*Shanghai Jiao Tong University, Shanghai 200240, People's Republic of China*
[49]*Shanxi Normal University, Linfen 041004, People's Republic of China*
[50]*Shanxi University, Taiyuan 030006, People's Republic of China*
[51]*Sichuan University, Chengdu 610064, People's Republic of China*
[52]*Soochow University, Suzhou 215006, People's Republic of China*
[53]*South China Normal University, Guangzhou 510006, People's Republic of China*
[54]*Southeast University, Nanjing 211100, People's Republic of China*
[55]*State Key Laboratory of Particle Detection and Electronics,*
Beijing 100049, Hefei 230026, People's Republic of China
[56]*Sun Yat-Sen University, Guangzhou 510275, People's Republic of China*
[57]*Suranaree University of Technology, University Avenue 111, Nakhon Ratchasima 30000, Thailand*
[58]*Tsinghua University, Beijing 100084, People's Republic of China*
[59a]*Turkish Accelerator Center Particle Factory Group, Istinye University, 34010 Istanbul, Turkey*
[59b]*Near East University, Nicosia, North Cyprus, Mersin 10, Turkey*
[60]*University of Chinese Academy of Sciences, Beijing 100049, People's Republic of China*
[61]*University of Groningen, NL-9747 AA Groningen, The Netherlands*
[62]*University of Hawaii, Honolulu, Hawaii 96822, USA*
[63]*University of Jinan, Jinan 250022, People's Republic of China*
[64]*University of Manchester, Oxford Road, Manchester M13 9PL, United Kingdom*
[65]*University of Muenster, Wilhelm-Klemm-Strasse 9, 48149 Muenster, Germany*
[66]*University of Oxford, Keble Road, Oxford OX13RH, United Kingdom*
[67]*University of Science and Technology Liaoning, Anshan 114051, People's Republic of China*
[68]*University of Science and Technology of China, Hefei 230026, People's Republic of China*
[69]*University of South China, Hengyang 421001, People's Republic of China*
[70]*University of the Punjab, Lahore-54590, Pakistan*
[71a]*University of Turin, I-10125 Turin, Italy*
[71b]*University of Eastern Piedmont, I-15121 Alessandria, Italy*
[71c]*INFN, I-10125 Turin, Italy*
[72]*Uppsala University, Box 516, SE-75120 Uppsala, Sweden*
[73]*Wuhan University, Wuhan 430072, People's Republic of China*
[74]*Xinyang Normal University, Xinyang 464000, People's Republic of China*
[75]*Yantai University, Yantai 264005, People's Republic of China*
[76]*Yunnan University, Kunming 650500, People's Republic of China*
[77]*Zhejiang University, Hangzhou 310027, People's Republic of China*
[78]*Zhengzhou University, Zhengzhou 450001, People's Republic of China*

[a]Also at the Moscow Institute of Physics and Technology, Moscow 141700, Russia.
[b]Also at the Novosibirsk State University, Novosibirsk 630090, Russia.
[c]Also at the NRC "Kurchatov Institute," PNPI, 188300 Gatchina, Russia.
[d]Also at Goethe University Frankfurt, 60323 Frankfurt am Main, Germany.
[e]Also at Key Laboratory for Particle Physics, Astrophysics and Cosmology, Ministry of Education; Shanghai Key Laboratory for Particle Physics and Cosmology; Institute of Nuclear and Particle Physics, Shanghai 200240, People's Republic of China.
[f]Also at Key Laboratory of Nuclear Physics and Ion-beam Application (MOE) and Institute of Modern Physics, Fudan University, Shanghai 200443, People's Republic of China.
[g]Also at State Key Laboratory of Nuclear Physics and Technology, Peking University, Beijing 100871, People's Republic of China.
[h]Also at School of Physics and Electronics, Hunan University, Changsha 410082, China.
[i]Also at Guangdong Provincial Key Laboratory of Nuclear Science, Institute of Quantum Matter, South China Normal University, Guangzhou 510006, China.
[j]Also at Frontiers Science Center for Rare Isotopes, Lanzhou University, Lanzhou 730000, People's Republic of China.
[k]Also at Lanzhou Center for Theoretical Physics, Lanzhou University, Lanzhou 730000, People's Republic of China.
[l]Also at the Department of Mathematical Sciences, IBA, Karachi, Pakistan.

A determination of the *CP*-even fraction F_+ in the decay $D^0 \to K^+ K^- \pi^+ \pi^-$ is presented. Using 2.93 fb^{-1} of $e^+ e^- \to \psi(3770) \to D\bar{D}$ data collected by the BESIII detector, one charm meson is reconstructed in the signal mode and the other in a *CP* eigenstate or the decay $D \to K^0_{S,L} \pi^+ \pi^-$. Analysis of the relative rates of these double-tagged events yields the result $F_+ = 0.730 \pm 0.037 \pm 0.021$, where the first uncertainty is statistical and the second is systematic. This is the first model-independent measurement of F_+ in $D^0 \to K^+ K^- \pi^+ \pi^-$ decays.

I. INTRODUCTION

The Standard Model description of *CP* violation may be tested by measuring the lengths and angles of the unitary triangle of the Cabibbo-Kobayashi-Maskawa (CKM) matrix [1,2]. One of these angles, commonly denoted by γ [3], is the only one accessible through tree-level processes, with negligible theoretical uncertainties [4]. Thus, a precise determination of γ is an excellent Standard Model benchmark and direct measurements of γ can be compared with indirect measurements that may be sensitive to new physics at loop level.

The angle γ is conventionally measured in $B^\pm \to DK^\pm$ decays, where D is a superposition of the flavor eigenstates D^0 and $\overline{D^0}$. An important class of D-meson decays for this purpose are those to *CP* eigenstates [5]. Similarly, one can also use decay modes with mixed *CP* content to measure γ, provided that this content is known [6,7]. This content is parametrized by F_+, the *CP*-even fraction of the decay. Furthermore, decay modes with mixed *CP* content can be used in studies of D^0–$\overline{D^0}$ oscillations, and searches for *CP* violation in the charm system [8].

This paper presents the first model-independent measurement of the *CP*-even fraction F_+ for the decay $D^0 \to K^+ K^- \pi^+ \pi^-$ using 2.93 fb^{-1} of quantum-correlated $\psi(3770) \to D\bar{D}$ data collected by the BESIII experiment. This measurement complements other strong-phase measurements performed with data collected by CLEO-c [7,9,10] and BESIII [11–14], and it is an important input to future analyses of γ and D^0-$\bar{D}^0$ oscillations using this channel.

II. MEASUREMENT STRATEGY

The strong decay of $\psi(3770) \to D\bar{D}$ conserves the $C = -1$ quantum number of the initial state, leaving the D-meson pair in an antisymmetric wave function. This quantum correlation allows for a direct access to the strong-phase difference between D^0 and $\bar{D}^0$ decays through a double-tag (DT) analysis. The method uses single-tag (ST) events, which are events where one of the charm mesons is reconstructed in a *CP* eigenstate, with no requirements on the decay of the other meson, and DT events, where both D mesons are reconstructed, one in a tag mode and the other in the signal mode.

Table I lists all the tag modes used for this analysis. The analysis can be split into three categories: *CP* tags, $K^0_S \pi^+ \pi^-$, and $K^0_L \pi^+ \pi^-$. The *CP* tags are modes in which the D meson decays to a *CP* eigenstate. The modes $D \to K^0_{S,L} \pi^+ \pi^-$ are of mixed *CP* content, since these decays can proceed through both *CP*-even and *CP*-odd amplitudes. The mode $\pi^+ \pi^- \pi^0$ is listed as a *CP*-even tag since its *CP*-even fraction, $F^{\pi\pi\pi^0}_+ = 0.973 \pm 0.017$ [7], is very close to unity. The modes $D \to K^0_L \pi^0 \pi^0$, $D \to K^0_L \omega$, and the self-tag $D \to K^+ K^- \pi^+ \pi^-$ have not been included because their yields are low and the inclusion of these tag modes would not significantly improve the precision of the measurement.

The predicted ST yield of a tag mode $D \to f$ with *CP*-even fraction F^f_+ is given by

$$N^{\mathrm{ST}}(f) = 2 N_{D\bar{D}} \mathcal{B}(f) \epsilon_{\mathrm{ST}}(f)(1 - (2F^f_+ - 1)y), \quad (1)$$

where $N_{D\bar{D}} = (10597 \pm 28 \pm 98) \times 10^3$ [15] is the total number of $D\bar{D}$ pairs, $\mathcal{B}$ is the branching fraction, ϵ_{ST} is the reconstruction efficiency of the ST mode, and $y = (0.615^{+0.056}_{-0.055}) \times 10^{-2}$ is the charm-mixing parameter [16].

TABLE I. Tag modes used in this analysis.

Category	Tag modes
CP even	$K^+ K^-$, $\pi^+ \pi^-$, $K^0_S \pi^0 \pi^0$, $\pi^+ \pi^- \pi^0$, $K^0_L \pi^0$
CP odd	$K^0_S \pi^0$, $K^0_S \eta_{\gamma\gamma}$, $K^0_S \eta'(\pi\pi\eta)$, $K^0_S \eta'(\rho^0 \gamma)$, $K^0_S \omega$
Mixed *CP*	$K^0_S \pi^+ \pi^-$, $K^0_L \pi^+ \pi^-$

In Eq. (1) and subsequent expressions, $\mathcal{O}(y^2)$ terms are neglected. For pure *CP*-even (odd) tags, $F_+^f = 1$ (0).

Events where one D meson is reconstructed as the signal decay $D \to K^+ K^- \pi^+ \pi^-$, while the other is reconstructed as a pure or mixed-*CP* tag mode f, have a predicted DT yield

$$N^{\mathrm{DT}}(KK\pi\pi|f) = 2N_{D\bar{D}}\mathcal{B}(f)\mathcal{B}(KK\pi\pi)\epsilon_{\mathrm{DT}}(KK\pi\pi|f)$$
$$\times (1 - (2F_+^f - 1)(2F_+ - 1)), \qquad (2)$$

where $\mathcal{B}(KK\pi\pi)$ is the branching fraction of $D^0 \to K^+ K^- \pi^+ \pi^-$, ϵ_{DT} is the reconstruction efficiency of the DT event, and F_+ denotes the *CP*-even fraction of $D^0 \to K^+ K^- \pi^+ \pi^-$. Equations (1) and (2) can be combined into

$$\frac{N^{\mathrm{DT}}(KK\pi\pi|f)}{N^{\mathrm{ST}}(f)/(1 - (2F_+^f - 1)y)} \times \frac{\epsilon_{\mathrm{ST}}(f)}{\epsilon_{\mathrm{DT}}(KK\pi\pi|f)}$$
$$= \mathcal{B}(KK\pi\pi)(1 - (2F_+^f - 1)(2F_+ - 1)). \qquad (3)$$

Equation (3) indicates that the ratio of the DT to ST yields, after efficiency corrections, is sensitive to $\mathcal{B}(KK\pi\pi)$ and the *CP*-even fraction F_+. Measuring this quantity for tags of different *CP* eigenvalues allows F_+ to be determined.

For the $K_S^0 \pi^+ \pi^-$ tag, which is a decay mode of mixed *CP*, an enhanced sensitivity to F_+ is obtained by separating events into bins of phase space of the tag decay. The amplitude-averaged strong-phase difference between D^0 and $\bar{D}^0$ decays has been measured in these bins by both CLEO [17] and BESIII [11]. The binning scheme used for this analysis is the "equal $\Delta\delta_D$ binning," where bin boundaries are chosen such that each bin spans an equal range in the strong-phase difference. The fractional yield K_i of D^0 decays and amplitude-averaged cosine of the strong-phase difference c_i have been measured in each bin. There are eight pairs of bins in total [17], and since each pair of bins have the same value for c_i, the data in each pair are merged. The combined CLEO and BESIII results from Ref. [11] are used, and they are treated as external inputs to the F_+ determination. The yield-ratio expression in bin i is

$$\frac{N_i^{\mathrm{DT}}(KK\pi\pi|f)}{N^{\mathrm{ST}}(f)/(1 - (2F_+^f - 1)y)} \times \frac{\epsilon_{\mathrm{ST}}(f)}{\epsilon_{\mathrm{DT}}(KK\pi\pi|f)}$$
$$= \mathcal{B}(KK\pi\pi)(K_i + K_{-i} - 2\sqrt{K_i K_{-i}} c_i (2F_+ - 1)). \quad (4)$$

The expression for the $D \to K_L^0 \pi^+ \pi^-$ tag is obtained by replacing K_i with K_i' and c_i with $-c_i'$, the values of which are also reported in Refs. [11,17].

III. BEPCII AND THE BESIII DETECTOR

The BESIII detector [18] records symmetric e^+e^- collisions provided by the BEPCII storage ring [19], which operates with a center-of-mass energy range from $\sqrt{s} = 2.00$ to 4.95 GeV, with a peak luminosity of 1×10^{33} cm^{-2} s^{-1} achieved at $\sqrt{s} = 3.773$ GeV. BESIII has collected large data samples in this energy region [20]. The cylindrical core of the BESIII detector covers 93% of the full solid angle and consists of a helium-based multilayer drift chamber (MDC), a plastic scintillator time-of-flight system (TOF), and a CsI(Tl) electromagnetic calorimeter (EMC), which are all enclosed in a superconducting solenoidal magnet providing a 1.0 T magnetic field. The solenoid is supported by an octagonal flux-return yoke with resistive plate counter muon-identification modules interleaved with steel. The charged-particle momentum resolution at 1 GeV/c is 0.5%, and the resolution of the rate of energy loss, dE/dx, is 6% for electrons from Bhabha scattering. The EMC measures photon energies with a resolution of 2.5% (5%) at 1 GeV in the barrel (end cap) region. The time resolution in the TOF barrel region is 68 ps, while that in the end cap region is 110 ps.

Simulated data samples produced with a GEANT4-based [21] Monte Carlo (MC) package, which includes the geometric description of the BESIII detector and the detector response, are used to determine detection efficiencies and to estimate backgrounds. The simulation models the beam-energy spread and initial-state radiation in the e^+e^- annihilations with the generator KKMC [22]. The inclusive MC sample includes the production of $D\bar{D}$ pairs, the non-$D\bar{D}$ decays of the $\psi(3770)$, the initial-state radiation production of the J/ψ and $\psi(3686)$ states, and the continuum processes incorporated in KKMC [22]. All particle decays are modelled with EvtGen [23,24] using branching fractions either taken from the Particle Data Group [25], when available, or otherwise estimated with LUNDCHARM [26,27]. Final-state radiation from charged final-state particles is incorporated using the PHOTOS package [28].

To ensure the best possible description of the distribution of the $D \to K^+ K^- \pi^+ \pi^-$ decays in phase space, the simulation samples are reweighted using the most recent amplitude model for this decay [29]. Quantum correlations are accounted for in the reweighting.

IV. EVENT SELECTION

Charged tracks detected in the MDC are required to be within a polar angle (θ) range of $|\cos\theta| < 0.93$, where θ is defined with respect to the z axis, which is the symmetry axis of the MDC. For charged tracks not originating from K_S^0 decays, the distance of closest approach to the interaction point (IP), $|V_z|$, must be less than 10 cm along the z axis, and less than 1 cm in the transverse plane.

Photon candidates are identified using showers in the EMC. The deposited energy of each shower must be more than 25 MeV in the barrel region ($|\cos\theta| < 0.80$) and more than 50 MeV in the end cap region ($0.86 < |\cos\theta| < 0.92$). To exclude showers that originate from charged tracks, the angle subtended by the EMC shower and the position of the closest charged track at the EMC must be greater than 10 degrees as measured from the IP. To suppress electronic noise and showers unrelated to the event, the difference between the EMC time and the event-start time is required to be within [0, 700] ns.

Particle identification for charged tracks combines measurements of the dE/dx in the MDC, and the time of flight as measured by the TOF system, to form likelihoods $\mathcal{L}(h)$ for each hadron hypothesis h ($h = K, \pi$). Charged kaons and pions are identified by comparing the likelihoods for the kaon and pion hypotheses, $\mathcal{L}(K) > \mathcal{L}(\pi)$ and $\mathcal{L}(\pi) > \mathcal{L}(K)$, respectively.

Each K_S^0 candidate is reconstructed from two oppositely charged tracks satisfying $|V_z| < 20$ cm. The two charged tracks are assigned the pion hypothesis without imposing particle identification criteria. They are constrained to originate from a common vertex and are required to have an invariant mass within 12 MeV/c^2 of the known K_S^0 mass [25]. The decay length of the K_S^0 candidate is required to be greater than twice the vertex resolution away from the IP.

Candidate π^0 and η mesons are reconstructed through the decays $\pi^0 \to \gamma\gamma$ and $\eta \to \gamma\gamma$, with their diphoton invariant masses required to be within [115, 150] and [480, 580] MeV/c^2, respectively. The η' meson is reconstructed through $\eta' \to \pi^+\pi^-\eta$ and $\rho^0(\pi^+\pi^-)\gamma$, with the invariant masses of the decay products within [940, 976] and [940, 970] MeV/c^2. The invariant mass of the pion pair in the ρ^0 decay must lie within [626, 924] MeV/c^2.

In the reconstruction of $D \to \pi^+\pi^-\pi^0$ and $D \to K^+K^-\pi^+\pi^-$ decays, the $\pi^+\pi^-$ pair is required to originate from a vertex within twice the vertex resolution from the IP in order to reduce backgrounds from $D \to K_S^0\pi^0$ and $D \to K_S^0K^+K^-$, respectively. For $\pi^+\pi^-\pi^0$, the $\pi^+\pi^-$ invariant mass is required to be more than 18 MeV/c^2 away from the known K_S^0 mass. For $K^+K^-\pi^+\pi^-$, the $\pi^+\pi^-$ mass must fall outside [477, 507] MeV/c^2.

For fully reconstructed tags, $\Delta E = E_D - \sqrt{s}/2$, where E_D is the reconstructed energy of the D meson, is required to be within 3σ of the signal peak. This requirement removes combinatorial background. In the tags containing a K_L^0, a partial reconstruction is performed where the signal $D \to K^+K^-\pi^+\pi^-$ is first reconstructed. From the remaining tracks and showers, the tag mode is reconstructed without the K_L^0 meson. It is required that there are no additional charged tracks or π^0 candidates. The K_L^0 momentum is then inferred from the missing momentum of the event. Since there is a missing particle, the ST yield cannot be measured in tag modes containing a K_L^0 meson.

Additionally, to increase the yield of $K^+K^-\pi^+\pi^-$ vs $K_S^0\pi^+\pi^-$ DTs, events where a charged kaon is not reconstructed are also considered. The tag mode $D \to K_S^0\pi^+\pi^-$ is first reconstructed, and it is required that there are exactly three remaining tracks, identified as a kaon and two oppositely charged pions. The momentum of the charged kaon that is not reconstructed is inferred from the missing momentum. To reduce the background from $D \to K^-\pi^+\pi^-\pi^+\pi^0$ decays, it is required that there are no π^0 candidates in the event.

In the $K_{S,L}^0\pi^+\pi^-$ tags, a Kalman kinematic fit [30] is performed to improve the resolution of the final-state particle momenta by constraining the $K_{S,L}^0$ and D invariant masses to their known values [25].

V. SINGLE- AND DOUBLE-TAG YIELD DETERMINATION

The ST yield of each fully reconstructed tag mode is determined by a maximum-likelihood fit of the beam-constrained mass $M_{BC} = \sqrt{E_{\text{beam}}^2 - |\sum_i \vec{p}_i|^2}$, where the sum runs over the momenta $\vec{p}_i$ of all the D decay products. The signal shape is obtained from simulation, but convolved with a Gaussian function to account for differences in resolution between data and simulation. The width of the Gaussian function is a free parameter in the fit and the difference in resolution between data and simulation was found to be a few hundred keV/c^2. Since the difference is small, no further correction to the simulation is performed. The combinatorial background is modeled by an ARGUS function [31]. The M_{BC} distributions and the fitted shapes are shown in Fig. 1. In all cases the fit quality is found to be good.

For the partially reconstructed tag mode $D \to K_L^0\pi^0$, the ST yield cannot be measured directly. Nonetheless, an effective ST reconstruction efficiency is calculated from $\epsilon_{ST}(K_L\pi^0) = \epsilon_{DT}(KK\pi\pi|K_L\pi^0)/\epsilon_{ST}(KK\pi\pi)$. The effective ST yield is then calculated from this efficiency, the branching fraction [32], and $N_{D\bar{D}}$, using Eq. (1). The ST yields and their efficiencies, determined from simulation, are presented in Table II. The ST yields are in good agreement with the results from Refs. [11,12,14].

The level of peaking background in the fully reconstructed tag modes is around 1% or less. In tag modes containing a K_L^0 there is a larger contamination from $K_S^0 \to \pi^0\pi^0$ decays, where the π^0 mesons are not reconstructed. This peaking background is found from simulation to be around 6% of the signal yield. The shapes of peaking backgrounds are fixed from simulation samples, while the yields are calculated from the branching fractions and efficiencies, relative to that of the signal yield.

Similarly, for fully reconstructed DT events, the M_{BC} on the signal side is fitted. The approach is identical to that for ST candidates, but corrections are applied to the peaking-background estimates to account for enhancements and
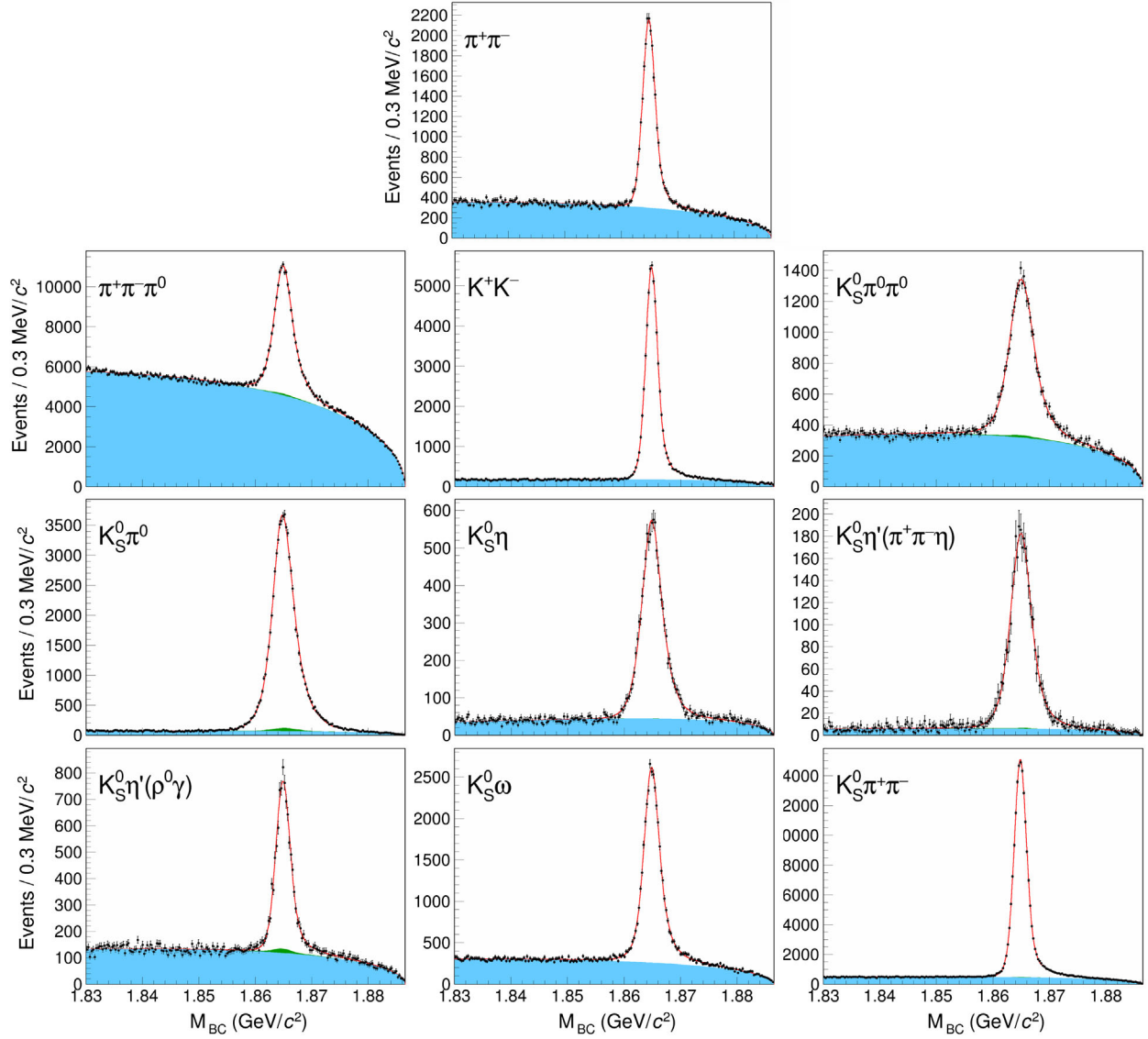
FIG. 1. ST M_{BC} distributions. Data points are shown in black with error bars and the red curve is the fit result. The solid blue shape is combinatorial background. The green, stacked on top of the blue, is peaking background.

TABLE II. ST yields and efficiencies for *CP* tags. In the case of modes involving K_L^0 mesons, these are effective quantities, as explained in the text. The uncertainties are statistical only.

Tag	Yield	Efficiency (%)
$K_S^0\omega$	22068 ± 217	14.50 ± 0.08
$K_S^0\eta'(\pi^+\pi^-\eta)$	3213 ± 62	12.81 ± 0.07
$K_S^0\eta'(\rho^0\gamma)$	8283 ± 116	20.80 ± 0.09
$K_S^0\eta$	9308 ± 113	31.78 ± 0.10
$K_S^0\pi^0$	67876 ± 278	38.18 ± 0.11
$\pi^+\pi^-\pi^0$	107504 ± 602	36.65 ± 0.11
$\pi^+\pi^-$	20386 ± 179	67.41 ± 0.10
$K_S^0\pi^0\pi^0$	22392 ± 229	14.35 ± 0.08
$K_L^0\pi^0$	47595 ± 1653	27.83 ± 0.23
K^+K^-	56303 ± 262	63.41 ± 0.11

suppressions due to quantum correlations. The quantum-correlation corrections are calculated using knowledge of the *CP* contents of both the signal and tag modes. The *CP* content of $D^0 \to K^+K^-\pi^+\pi^-$ is obtained from the amplitude model in Ref. [29].

For partially reconstructed tag modes, a fit of the missing-mass squared M_{miss}^2 of the missing particle is performed instead. In the $K_{S,L}^0\pi^+\pi^-$ tag modes, which are split into bins of phase space, a simultaneous fit is performed where the signal-shape parameters are shared between all bins, while the yield of signal and combinatorial backgrounds are varied independently in each bin. Figure 2 shows the signal M_{BC} distributions of fully reconstructed modes in data, along with the fitted shapes. The corresponding M_{miss}^2 distributions for partially reconstructed modes are shown in Fig. 3. For the $K_{S,L}^0\pi^+\pi^-$ tags,
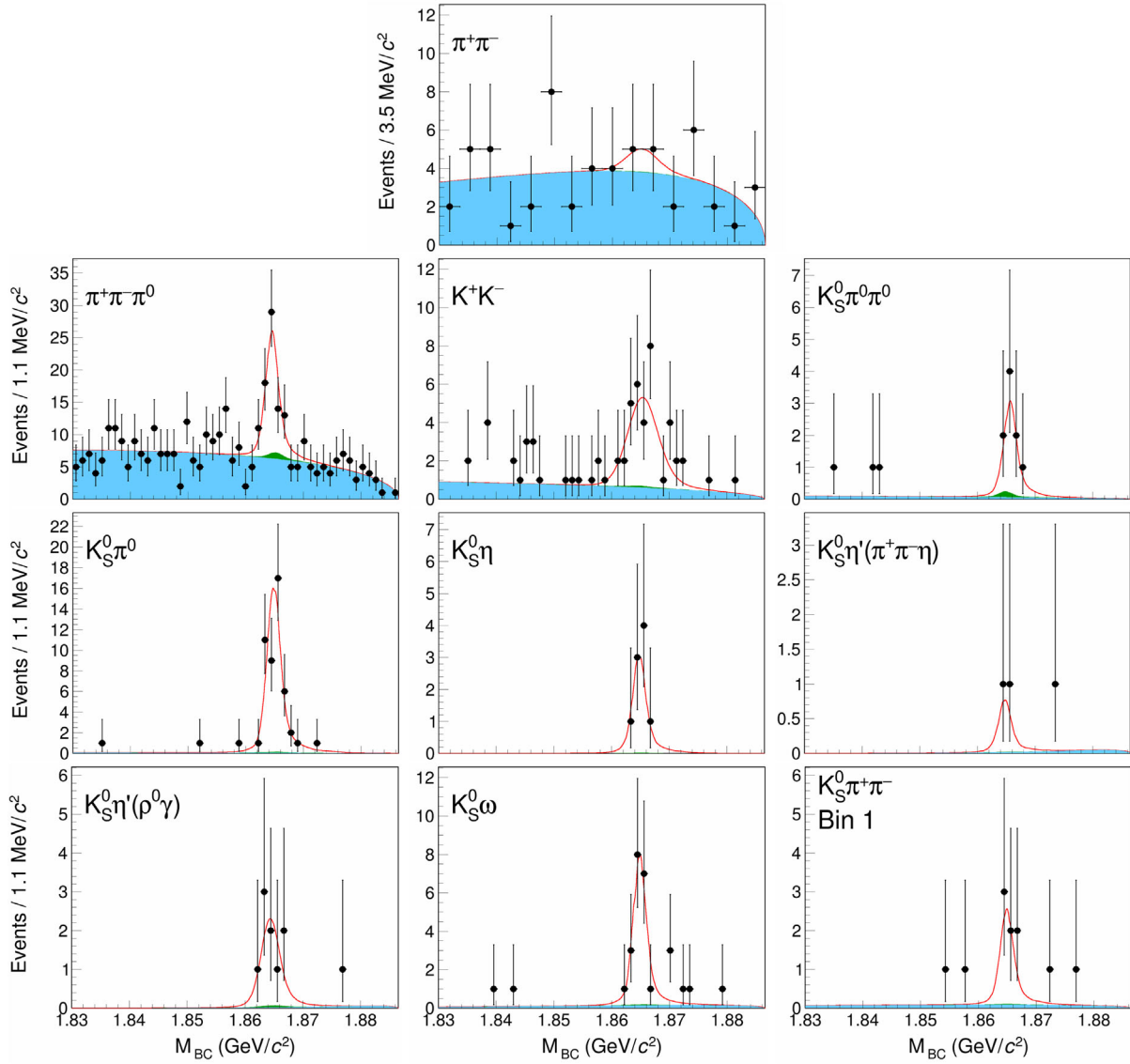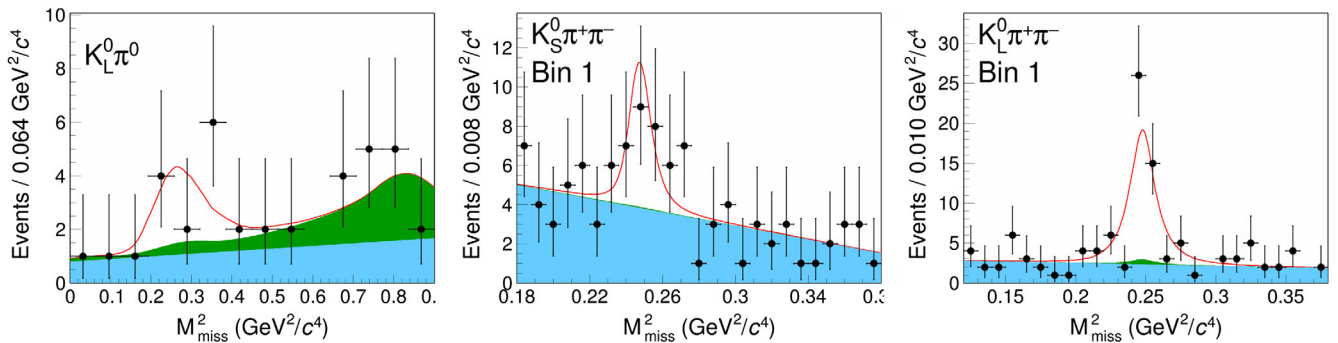
FIG. 2.   DT M_{BC} distributions of fully reconstructed DT candidates. Data points are shown in black with error bars and the red curve is the fit result. The solid blue shape is combinatorial background. The green, stacked on top of the blue, is peaking background.

FIG. 3.   DT M_{miss}^2 distributions of partially reconstructed DT candidates. Data points are shown in black with error bars and the red curve is the fit result. The solid blue shape is combinatorial background. The green, stacked on top of the blue, is peaking background.

TABLE III. DT yields and efficiencies for *CP* tags. The uncertainties are statistical only.

Tag mode	Yield	Efficiency (%)
$K_S^0\omega$	9 ± 3	2.23 ± 0.02
$K_S^0\eta'(\pi^+\pi^-\eta)$	2 ± 2	2.02 ± 0.02
$K_S^0\eta'(\rho^0\gamma)$	9 ± 3	3.29 ± 0.03
$K_S^0\eta$	9 ± 3	5.72 ± 0.04
$K_S^0\pi^0$	48 ± 7	6.86 ± 0.04
$\pi^+\pi^-\pi^0$	53 ± 10	7.67 ± 0.04
$\pi^+\pi^-$	2 ± 4	15.07 ± 0.06
$K_S^0\pi^0\pi^0$	8 ± 3	2.87 ± 0.03
$K_L^0\pi^0$	7 ± 5	5.30 ± 0.04
K^+K^-	28 ± 10	14.55 ± 0.06

TABLE IV. DT yields for $K_{S,L}^0\pi^+\pi^-$ tags, for full and partial reconstruction, in bins of phase space. The global efficiencies are also shown. The uncertainties are statistical only.

	$K_S^0\pi^+\pi^-$	$K_S^0\pi^+\pi^-$	$K_L^0\pi^+\pi^-$
Bin	Full	Partial	Partial
1	7 ± 3	17 ± 7	45 ± 8
2	11 ± 4	4 ± 4	15 ± 5
3	5 ± 2	12 ± 6	19 ± 5
4	7 ± 3	0 ± 3	5 ± 3
5	11 ± 3	23 ± 7	11 ± 5
6	6 ± 2	7 ± 4	15 ± 4
7	12 ± 3	22 ± 6	22 ± 5
8	11 ± 4	6 ± 5	25 ± 6
Total	69 ± 9	91 ± 15	158 ± 15
$\epsilon_{\rm DT}$ (%)	6.56 ± 0.04	7.01 ± 0.04	7.25 ± 0.04

only the result in one bin of phase space is shown, but the other bins are very similar. The fitted yields and their efficiencies, as determined from simulation, are listed in Tables III and IV.

In the $D \to K_S^0\omega$ tag, there is also nonresonant $D \to K_S^0\pi^+\pi^-\pi^0$ background. To isolate $D \to K_S^0\omega$ candidates from nonresonant $D \to K_S^0\pi^+\pi^-\pi^0$, first the sPlot technique [33] is used on the $M_{\rm BC}$ variable to remove the flat combinatorial background. Then a fit of the $\pi^+\pi^-\pi^0$ invariant mass, after applying sWeights, is performed to obtain the yield of $K_S^0\omega$. This procedure is done with both ST and DT candidates.

VI. *CP*-EVEN FRACTION MEASUREMENT

A maximum-likelihood fit is performed to the ST and DT yields of *CP* tags listed in Tables II and III, respectively, assuming the relation given by Eq. (3). The uncertainties are assumed to follow a Gaussian distribution. The branching fraction $\mathcal{B}(KK\pi\pi)$ and the *CP*-even fraction F_+ are free parameters in the fit. Figure 4 shows the ratio of DT yields
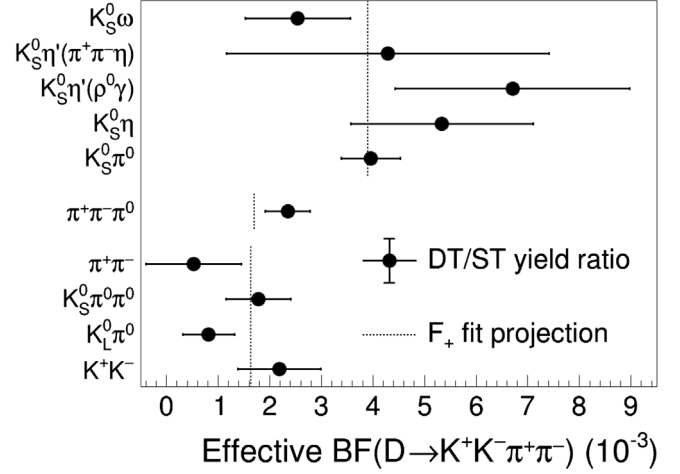

FIG. 4. The effective branching fraction (BF) of $D \to K^+K^-\pi^+\pi^-$ measured against *CP*-odd (top), $D \to \pi^+\pi^-\pi^0$ and *CP*-even (bottom) tags. The black dotted lines indicate the values expected from the fit.

to ST yields for each tag after efficiency corrections. Physically, this represents the effective branching fraction of $D \to K^+K^-\pi^+\pi^-$, where the D meson is prepared in a *CP* eigenstate. The fitted *CP*-even fraction is $F_+ = 0.704 \pm 0.042 \pm 0.028$, where the first uncertainty is from the statistical uncertainties of ST and DT yields and the second uncertainty is the systematic uncertainty, discussed in Sec. VII. The obtained branching fraction is $\mathcal{B}(KK\pi\pi) = (2.8 \pm 0.3) \times 10^{-3}$, where the uncertainty is statistical. It is consistent with the current value from the Particle Data Group [25].

Similarly, a maximum-likelihood fit is performed using Eq. (4) and the $K_{S,L}^0\pi^+\pi^-$ results from Table IV. Table IV contains the global reconstruction efficiencies, but in the fit a full 8×8 efficiency matrix is used to account for both the reconstruction efficiency in each bin, and the migration of events between the bins. The bin-migration effect is between 2%–14% for the fully reconstructed $K_S^0\pi^+\pi^-$ mode, 3%–15% for the partially reconstructed $K_S^0\pi^+\pi^-$ mode and 4%–24% for the $K_L^0\pi^+\pi^-$ mode.

Because the branching fraction of $D \to K_L^0\pi^+\pi^-$ is currently unknown, $\mathcal{B}(KK\pi\pi)$ is a free parameter and varied independently for the $K_S^0\pi^+\pi^-$ and $K_L^0\pi^+\pi^-$ tags. It is therefore not necessary to normalize the DT yield of the $D \to K_L^0\pi^+\pi^-$ tag with the corresponding ST yields and thus the measured $\mathcal{B}(KK\pi\pi)$ carry no useful information. For the $D \to K_S^0\pi^+\pi^-$ tag, the fitted branching fraction is $\mathcal{B}(KK\pi\pi) = (2.3 \pm 0.3) \times 10^{-3}$, where the uncertainty is statistical, which is compatible with both the known value and with the result from the *CP* tags.

Figure 5 shows the DT yields in bins of phase space, where the sum of the yields has been normalized to unity. The $K_S^0\pi^+\pi^-$ plot contains both the fully reconstructed and
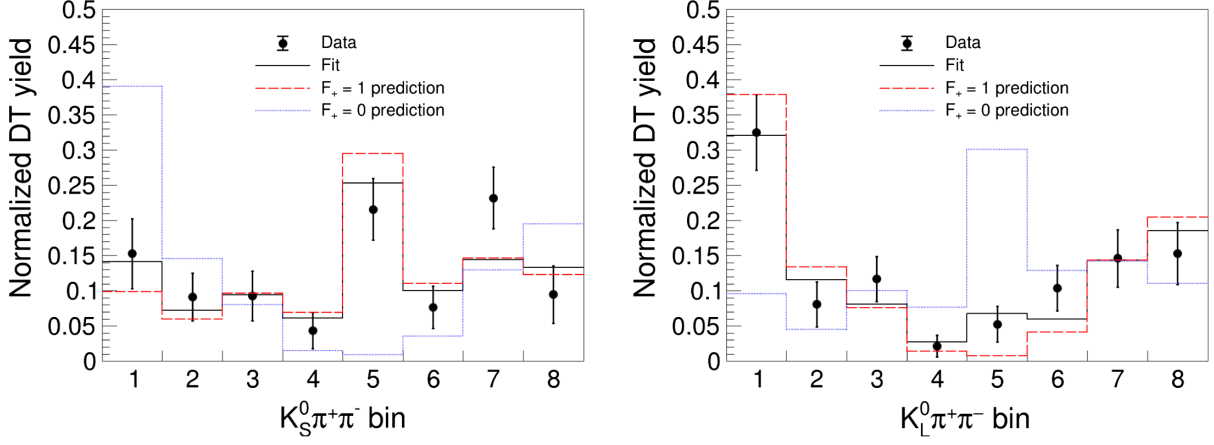
FIG. 5.   Fit results for the $K^0_{S,L}\pi^+\pi^-$ tags. Also shown is the fit projection, and the predictions for $F_+ = 1$ and $F_+ = 0$.

partially reconstructed $K^+K^-\pi^+\pi^-$ vs $K^0_S\pi^+\pi^-$ data. The fit of $K^0_{S,L}\pi^+\pi^-$ results in $F_+ = 0.798 \pm 0.077 \pm 0.019$, which is consistent with the value obtained from CP tags.

The combined measurement of the CP-even fraction, using both CP tags and $K^0_{S,L}\pi^+\pi^-$ tags, and taking into account all correlations, is $F_+ = 0.730 \pm 0.037 \pm 0.021$. This result is in agreement with the central value $F_+ = 0.736$ predicted by the model of Ref. [29].

VII. SYSTEMATIC UNCERTAINTIES

Several sources of systematic uncertainties in the F_+ measurement are considered. The assigned values are given in Table V, listed separately for the CP tags and the $K^0_{S,L}\pi^+\pi^-$ tags.

Since the efficiencies are calculated from simulation samples of finite size, there are statistical uncertainties associated with their values. For the CP tags, the efficiency corrections are single numbers, but in the case of the $K^0_{S,L}\pi^+\pi^-$ tags the efficiency corrections are matrices that also account for bin migration. To estimate the effect on F_+, the fit described in Sec. VI is repeated 1000 times, each

TABLE V.   Summary of the sources of systematic uncertainty in the measurement of F_+, multiplied by 10^2. Entries marked "/" indicate that the source is not relevant for the decay mode. The last two entries are fully correlated between the two classes of tag.

Source	CP tags	$K^0_{S,L}\pi^+\pi^-$ tags
MC sample size	0.1	0.4
$K^0_L\pi^0$ ST yield	2.1	/
Efficiency factorization	0.6	/
External inputs	0.3	0.8
ST and DT yields	0.2	0.3
K^0_S veto	0.8	0.8
Efficiency reweighting	1.0	1.0
Total	2.6	1.6

time smearing the efficiencies and efficiency matrices. The smearing of a parameter is performed by adding a random number, drawn from a Gaussian distribution with zero mean and a width equal to the uncertainty, to the parameter. The resulting width of the fitted F_+ values is taken as the systematic uncertainty.

The form of Eqs. (3) and (4) makes the analysis insensitive to biases arising from any imperfections in the modeling of the particle-reconstruction efficiencies in the MC simulation for the tag modes. Similarly, the determination of F_+ is robust against these same imperfections affecting the signal decay. The case of the $K^0_L\pi^0$ tag requires separate consideration. Here its effective ST yield has an uncertainty associated with the knowledge of the branching fraction and $N_{D\bar{D}}$. The value of the branching fraction that is input to the analysis derives from the measurement in Ref. [32], which was performed on the same dataset using a DT method. The systematic uncertainties associated with the π^0 reconstruction and the track veto in this measurement are common with the current analysis and hence cancel. The relative uncertainty on the branching fraction, with these contributions removed, is 3.3%. This uncertainty, together with that on $N_{D\bar{D}}$, is propagated to the determination of F_+ by smearing the $K^0_L\pi^0$ effective ST yield.

When the CP-tags yields are corrected for their efficiencies, it is implicitly assumed that the DT efficiencies factorize into a product of ST efficiencies in the same manner for all tags. The imperfections in this assumption are studied by repeating the determination of F_+ with all DT efficiencies replaced by a product of ST efficiencies. The resulting bias in F_+ is assigned as the systematic uncertainty arising from this factorization assumption.

In the fit of CP tags, the $\pi^+\pi^-\pi^0$ tag mode requires an external input for its CP-even fraction $F_+^{\pi\pi\pi^0}$ [7]. Similarly, the fit of the $K^0_{S,L}\pi^+\pi^-$ tags requires external inputs for the K_i and c_i parameters [11,17]. The systematic uncertainties arising from external inputs are estimated by smearing

these parameters. The correlations are also accounted for in the smearing of the c_i values.

In the determination of the ST and DT yields, there are systematic uncertainties arising from the peaking-background yields and the mass-shape parametrization. It is found that the choice of parametrization of the mass shapes has a negligible effect on the systematic uncertainties. When estimating the peaking-background contributions, the measured branching fractions of both signal and background have associated uncertainties [25] that must be accounted for. In addition, the quantum-correlation corrections also have uncertainties due to imperfect knowledge of the *CP* contents. To propagate these to the measurement of F_+, the peaking-background yields are smeared in the fit described in Sec. V to first obtain a systematic uncertainty for the signal yields. Then the signal yields themselves are smeared in the F_+ fit to obtain the systematic uncertainty associated with the peaking backgrounds.

The K_S^0 veto removes 4% of the $D \to K^+ K^- \pi^+ \pi^-$ phase space, and thus can perturb F_+ from the value that corresponds to the inclusive decay. This potential bias is estimated by calculating F_+ using the model from Ref. [29] with and without the veto. The difference is assigned as the systematic uncertainty, which is common to both *CP* and $K_{S,L}^0 \pi^+ \pi^-$ tags.

Finally, there is a systematic uncertainty due to the efficiency reweighting that accounts for any discrepancies between the data and the amplitude model. With the current precision, it can be assumed that this systematic uncertainty is common between all tags. This systematic uncertainty originates from Eqs. (3) and (4), where it is seen that any imperfections in the modeling of the $D \to K^+ K^- \pi^+ \pi^-$ decay are not canceled in the ratio, unlike the efficiency of the tag-side decay. The effect is studied with a data-driven strategy by using samples of ST $D \to K^+ K^- \pi^+ \pi^-$ candidates in data and simulation. Five invariant-mass variables are compared between data and simulation. Any discrepancies between data and simulation are removed by reweighting the simulation samples. Using these weights, the fit of F_+ is repeated and the change in the result is assigned as the systematic uncertainty. Since this systematic uncertainty calculation is data-driven, improved precision is also expected with more data.

VIII. SUMMARY AND OUTLOOK

The first model-independent measurement of the *CP*-even fraction F_+ of the decay mode $D^0 \to K^+ K^- \pi^+ \pi^-$ has been performed using ten *CP*-eigenstate tags and the self-conjugate multibody modes $D \to K_{S,L}^0 \pi^+ \pi^-$ from a data sample of $e^+ e^- \to \psi(3770) \to D\bar{D}$ events corresponding to an integrated luminosity of 2.93 fb^{-1}. The results combine to $F_+ = 0.730 \pm 0.037 \pm 0.021$, where the first uncertainty is statistical and the second is systematic, indicating that this decay mode has a high *CP*-even content. This result will be valuable for future measurements of the CKM-angle γ, and studies of charm mixing and *CP* violation at LHCb and Belle II.

The measurement is dominated by statistical uncertainty and it will improve significantly with the larger charm-threshold dataset that BESIII is expected to collect in the coming years [20]. This increased sample size will also allow the study to be extended to localized regions of phase space, as has been done for other decay modes [9–13,17].

[1] N. Cabibbo, Phys. Rev. Lett. **10**, 531 (1963).

[2] M. Kobayashi and T. Maskawa, Prog. Theor. Phys. **49**, 652 (1973).

[3] Also denoted as ϕ_3 in the literature.

[4] J. Brod and J. Zupan, J. High Energy Phys. 01 (2014) 051.

[5] M. Gronau and D. Wyler, Phys. Lett. B **265**, 172 (1991).

[6] M. Nayak, J. Libby, S. Malde, C. Thomas, G. Wilkinson, R. A. Briere, P. Naik, T. Gershon, and G. Bonvicini, Phys. Lett. B **740**, 1 (2015).

[7] S. Malde, C. Thomas, G. Wilkinson, P. Naik, C. Prouve, J. Rademacker, J. Libby, M. Nayak, T. Gershon, and R. A. Briere, Phys. Lett. B **747**, 9 (2015).

[8] S. Malde, C. Thomas, and G. Wilkinson, Phys. Rev. D **91**, 094032 (2015).

[9] S. Harnew, P. Naik, C. Prouve, J. Rademacker, and D. Asner, J. High Energy Phys. 01 (2018) 144.

[10] P. K. Resmi, J. Libby, S. Malde, and G. Wilkinson, J. High Energy Phys. 01 (2018) 082.

[11] M. Ablikim *et al.* (BESIII Collaboration), Phys. Rev. D **101**, 112002 (2020).

[12] M. Ablikim *et al.* (BESIII Collaboration), Phys. Rev. D **102**, 052008 (2020).

[13] M. Ablikim *et al.* (BESIII Collaboration), J. High Energy Phys. 05 (2021) 164.

[14] M. Ablikim *et al.* (BESIII Collaboration), Phys. Rev. D **106**, 092004 (2022).

[15] M. Ablikim *et al.* (BESIII Collaboration), Chin. Phys. C **42**, 083001 (2018).

[16] Y. S. Amhis *et al.* (HFLAV Collaboration), Eur. Phys. J. C **81**, 226 (2021).

[17] J. Libby *et al.* (CLEO Collaboration), Phys. Rev. D **82**, 112006 (2010).

[18] M. Ablikim *et al.* (BESIII Collaboration), Nucl. Instrum. Methods Phys. Res., Sect. A **614**, 345 (2010).

[19] C. Yu *et al.*, in *Proceedings of the 7th International Particle Accelerator Conference* (The Joint Accelerator Conferences Website, Geneva, Switzerland, 2016), p. TUYA01.

[20] M. Ablikim *et al.* (BESIII Collaboration), Chin. Phys. C **44**, 040001 (2020).

[21] S. Agostinelli *et al.* (GEANT4 Collaboration), Nucl. Instrum. Methods Phys. Res., Sect. A **506**, 250 (2003).

[22] S. Jadach, B. Ward, and Z. Was, Comput. Phys. Commun. **130**, 260 (2000).

[23] D. Lange, Nucl. Instrum. Methods Phys. Res., Sect. A **462**, 152 (2001).

[24] R. G. Ping, Chin. Phys. C **32**, 599 (2008).

[25] R. L. Workman *et al.* (Particle Data Group), Prog. Theor. Exp. Phys. **2022**, 083C01 (2022).

[26] R. L. Yang, R. G. Ping, and H. Chen, Chin. Phys. Lett. **31**, 061301 (2014).

[27] J. C. Chen, G. S. Huang, X. R. Qi, D. H. Zhang, and Y. S. Zhu, Phys. Rev. D **62**, 034003 (2000).

[28] E. Richter-Was, Phys. Lett. B **303**, 163 (1993).

[29] R. Aaij *et al.* (LHCb Collaboration), J. High Energy Phys. 02 (2019) 126.

[30] W. D. Hulsbergen, Nucl. Instrum. Methods Phys. Res., Sect. A **552**, 566 (2005).

[31] H. Albrecht *et al.* (ARGUS Collaboration), Phys. Lett. B **241**, 278 (1990).

[32] M. Ablikim *et al.* (BESIII Collaboration), Eur. Phys. J. C **82**, 1009 (2022).

[33] M. Pivk and F. R. Le Diberder, Nucl. Instrum. Methods Phys. Res., Sect. A **555**, 356 (2005).